Journal of the European Ceramic Society 20 (2000) 1145–1152

Influence of residual and bridging stresses on the R-curve behavior of Mo- and FeAl-toughened alumina

O. Sbaizero[a,*], G. Pezzotti[b]

[a]Department of Materials Engineering, University of Trieste, Via Valerio 2, 34127 Trieste, Italy
[b]Department of Materials, Kyoto Institute of Technology, Matsugasaki, Sakyo-ku, Kyoto 606-8585, Japan

Received 30 March 1999; received in revised form 15 September 1999; accepted 8 October 1999

Abstract

Alumina matrix was toughened using either metal molybdenum or intermetallic FeAl particles. Mo and FeAl dispersoids were chosen because they have different thermomechanical properties (i.e. Young's modulus, Poisson ratio, as well as thermal expansion coefficient), giving rise to different residual stresses in the matrix. The R-curve behavior of these composites was first studied by stable-crack propagation experiments as a function of the volume fraction of dispersoid. The optimum fraction for toughening was different in the two composites: 25 and 15 vol% addition led to maximum toughness in the Mo- and FeAl added composite, respectively. This difference was ascribed to residual stresses. Microscopic observation of the crack path revealed, in both composites, the systematic presence of dispersoids acting as bridging sites in the crack wake, but only a few of them were plastically stretched. Residual stresses in the Al_2O_3 matrix, after sintering and microscopic bridging tractions during crack propagation, were quantitatively assessed using microprobe fluorescence spectroscopy. Bridging microstresses were assessed in situ by a linear map along the crack profile, at the critical condition for fracture propagation. Experimentally collected residual stresses and bridging stresses were discussed to explain the different fracture behavior of the composites.

Keywords: Al_2O_3; Composites; Inclusions; Residual stresses; Toughening

1. Introduction

Ceramic materials are good candidates for structural uses in which applications as lightweight high-temperature materials are required. However, their actual applications are largely limited by their intrinsic brittleness. To tackle this problem recent studies have been carried out with the aim of increasing ceramic toughness by producing ceramic composites. Among the possible matrices of these composites, alumina is very appealing because of its high melting point and hardness, as well as a good wear and friction behavior. Some successful attempts have been made to improve the alumina fracture toughness by adding a metallic phase. This topic has recently been the object of extensive theoretical assessments.[1,2] In these types of ceramic composites, often called cermets, many variables may be involved in the toughness improvement. Among them, very important roles are played by the morphology of the metallic phase and the microscopic distribution of residual stresses. Regarding the morphology of the metallic phase, it is possible to foresee two main cases: (i) the metal phase is dispersed in the matrix as isolated inclusions, and (ii) the metal phase is continuously interconnected at the grain boundaries of the matrix. Fracture mechanics studies[3,4] have shown that, independent of the morphology of the reinforcing phase, the main toughening mechanism arises from a bridging effect operated by the metallic ligaments stretched in the crack wake until they break.

In this study, we have focused our attention on a polycrystalline alumina matrix containing increasing fractions of either molybdenum metal or intermetallic FeAl which are both added as isolated dispersoids. According to the above arguments, dispersoid bridging should lead to a significant improvement in the crack resistance of the alumina matrix. Mo and FeAl dispersoids were chosen because despite having a similar morphology, they have different Young's moduli and thermal expansion coefficients (CTE). Therefore, after

* Corresponding author.
E-mail address: sbaizero@univ.trieste.it (O. Sbaizero).

0955-2219/00/$ - see front matter
PII: S0955-2219(99)00267-8

sintering the matrix should be affected by different residual stresses. Mo is a refractory hard metal (melting point = 2610°C) which retains high strength up to elevated temperatures. Its Young's modulus is close to that of the ceramic matrix and its thermal expansion coefficient is only slightly lower than that of alumina. FeAl has lower density and lower Young's modulus compared to Mo and, more importantly, its thermal expansion coefficient is much higher than that of alumina. In principle, FeAl should be essentially ductile at room temperature because as a BCC crystal it may show more than five independent slip systems. However, due to environmental embrittlement, atomic bond, bond polarization, and ordering, FeAl may also exhibit brittle fracture. Great efforts have been made to increase the FeAl room temperature ductility through the addition of some alloying elements such as Cr, Ti, Mg, B, Y. One notable result, showed by McKamey et al.,[5] is that the presence of soluted Cr significantly increases the FeAl ductility. For this reason, Cr-doped FeAl was used in the present study (Table 1).

The fracture behavior of Al_2O_3/Mo and Al_2O_3/FeAl model is investigated as a function of the volume fraction of the dispersoid. To clarify the fracture mechanisms, direct measurements of the microscopic bridging stresses, developed upon crack propagation, are assessed using in situ fluorescence spectroscopy. Due to insensitivity of metals and intermetallic phases to piezospectroscopic signals, fluorescence spectra are collected at the interface between the dispersoid and the Al_2O_3 matrix.[6] Residual stresses in the matrix, due to mismatch of thermoelastic properties between matrix and dispersoid, are also measured by fluorescence spectroscopy. The piezospectroscopic data are then used to relate the microscopic bridging stresses and the thermally induced residual stresses to the macroscopic fracture behavior of the ceramic composites.

2. Experimental procedures

2.1. Materials

High purity Al_2O_3 powder (AKP-53, Sumitomo Chemical Ltd., Japan) was mixed with either molybdenum particles (Japan New Metals Co., Japan. Average grain size = 2.6 μm) or FeAl particles (Centro Sviluppo Materiali, Italy. Average grain size = 3.0 μm). The FeAl powder contained: Cr = 4.2 wt%, C = 0.033 wt%, Zr = 22 ppm, B = 252 ppm, Y = 66 ppm. The weighted mixed powders were attrition milled in isopropyl alcohol for 4 h. Samples of each composite with fractions of second phase equal to 15 and 25 vol% were preformed by uniaxial pressing followed by cold isostatic pressing at 100 MPa. Hot-pressing of the composite samples was then performed in a graphite die, applying a pressure of 30 MPa for 20 min. Different hot-pressing temperatures of 1640 and 1245°C were selected for Al_2O_3/Mo and Al_2O_3/FeAl, respectively. The hot-pressing temperatures were selected according to the criterion of obtaining nearly full density of the composites with the minimum temperature. The samples were then slowly cooled down (200°C/h) to room temperature. The density of both types of composites, measured by the Archimede's method, was >99% of its theoretical value, calculated according to the rule of mixture. The average grain size of the matrix, assessed by image analysis from scanning electron micrographs, was in the range of 3.0–5.0 μm in both composites.

2.2. Fracture mechanics characterization

Specimens for fracture mechanics testing were bars 3×4×20 mm (B×W×L). A straight-through notch with a relative length, $a/W = 0.5$ was introduced at the center of the specimens by a diamond blade (thickness = 0.2 mm). Then, to reduce the influence of a finite notch-tip radius, the bottom part of the saw-notch was sharpened with a razor blade which was sprinkled with fine diamond paste. Using this procedure the notch root was sharpened to a radius of <5 μm. To achieve stable fracture propagation, in bending geometry, a crack stabilizer[7] for the three-point bending geometry was used (span = 16 mm). The load-displacement relation was directly measured with semiconductor strain gauges placed on the loading bar and on the tensile surface of the specimen, respectively. Further details of the notching procedure and the bending stabilizer have been reported elsewhere.[8,9] R-curve data were collected from the load-displacement curves obtained under a relatively fast cross-head speed of 0.1 mm/min. The crack length was concurrently measured by travelling optical microscopy during crack propagation. The crack resistance value, K_R relative to each visible crack extension was calculated from standard fracture mechanics equations.

2.3. Fluorescence spectroscopy

The Raman spectroscopic apparatus (ISA, T 64000 Jovin-Yvon) was used for measuring microscopic stresses as detected from the Cr^{3+} fluorescence bands of Al_2O_3.[10] An Ar-ion laser operating at a wavelength of 488 nm with a power of 300 mW was used as the excitation source, while an optical microscope was used both to focus the laser on the sample and to collect the scattered light. Light frequencies were analyzed using a triple monochromator equipped with a charge-coupled device camera. Residual stresses were measured in the Al_2O_3 phase with a laser spot of ≈50 μm placed on the bulk hot-pressed body. Such residual stresses arise from cooling down after hot-pressing due both to thermal expansion and elastic mismatch between the Al_2O_3

matrix and the dispersoid, as well as thermal anisotropy of the Al_2O_3 grain. The frequency shift due to the applied stress in $Al_2O_3$was monitored on the characteristic R_1, R_2 doublet (i.e. the two ruby fluorescence peaks located at 14400 and 14430 cm^{-1}, respectively). In the case of residual stress measurements, the frequency used as the standard value for zero stress was obtained from a monolithic Al_2O_3 hot-pressed body. The penetration depth of the laser beam below the specimen surface was experimentally calibrated and found to be ≈10 μm. A neon discharge lamp was used for obtaining an external frequency calibration, as well as temperature-dependent frequency shifts which were corrected by a standard calibration. In particular, using the R_2 line, whose piezo-spectroscopic anisotropy is much smaller than that of the R_1 line, the experimental error arising from using an average piezo-spectroscopic coefficient was minimized.

In the crack-profile maps experiments, a three-point bend loading jig was equipped with a load cell of 100 N and placed into the Raman apparatus. Profiles of stable propagating cracks were monitored in situ by optical microscopy. Concurrently, fluorescence spectra were recorded near the ceramic/metal interface of bridging sites both at zero external load and at the critical load for crack propagation. Fluorescence spectra in Al_2O_3 could be collected in ≈1 s, thus enabling in situ characterization during crack propagation. Since a large number of points had to be recorded under the same applied load, the load was temporarily arrested. However, no significant load-relaxation over such a holding time could be monitored. In these mapping experiments the dimension of the laser spot on the sample was ≈5 μm. To single out the actual bridging effect, without the influence of local residual stresses, the following experimental procedure was adopted. First, a linear map was recorded along the crack profile at zero external load. This map was used to establish the local ''zero-stress'' values of the fluorescence peak frequency. Then, a linear map was collected along the same crack but with the external load at the onset value for crack propagation. The neat (local) peak shifts were then calculated by subtracting at any location the frequency recorded at zero external load from that recorded at the onset load for fracture. The collected fluorescence data were analyzed with the curve-fitting algorithms included in the SpectraCalc software package (Galactic Industries Corp.). Local stresses at the monitored locations were calculated from the respective frequency shifts according to the piezo-spectroscopic coefficients, Π_c and Π_a given in the literature as 2.75 and 2.10 cm^{-1} GPa^{-1} for an *a*- and *c*-axis oriented sapphire crystal, respectively.[11] The average uniaxial piezo-spectroscopic coefficient $\Pi_u = (\Pi_c + 2\Pi_a)/3$ was employed to linearly relate the frequency shift ($\Delta\nu$) to the uniaxial bridging stress (σ_{BR}) according to the relation $\sigma_{BR} = \Pi_u \Delta\nu$. On the other hand, the triaxial state of stress due to thermal expansion and elastic mismatch between the constituent phases was evaluated using the average hydrostatic piezo-spectroscopy coefficient, $\Pi_t = (\Pi_c + 2\Pi_a)$.

3. Results

3.1. Microstructure and R-curve behavior

Scanning electron microscopy (SEM) pictures of the composites both containing 25 vol% of Mo or FeAl are shown in Fig. 1(a and b), respectively. From the viewpoint of the microstructural morphology, no obvious difference could be found between these two composites on the SEM scale. Only a few and very small (submicrometer) particles were dispersed within the alumina matrix grain, while the majority of the particles (> 1 μm) were located at grain boundaries, where they acted as grain growth inhibitors. The pre-cracked samples containing either 15 or 20 vol% showed no crack instability at any crack length when tested in bending geometry.

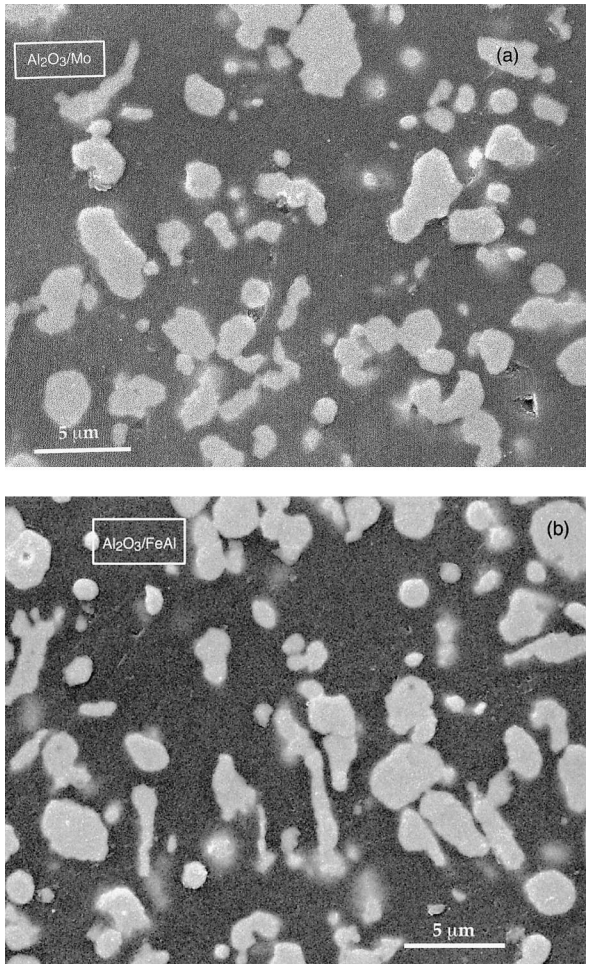

Fig. 1. SEM micrograph showing the 25 vol% composite microstructures: (a) Al_2O_3/Mo, (b) Al_2O_3/FeAl.

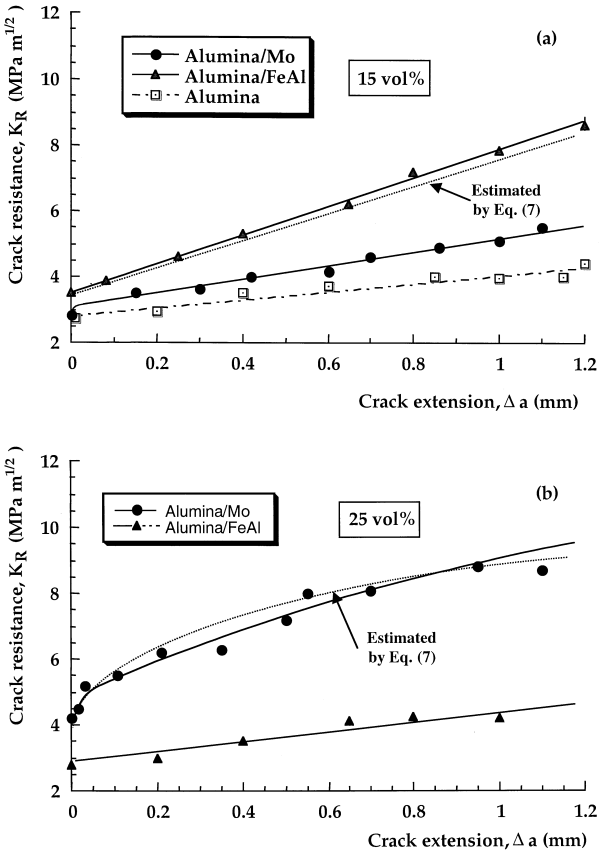

Fig. 2. R-curve behaviour of the composites investigated: (a) composites added with 15 vol% of dispersoid (b) comoposites added with 25 vol% of dispersoid. Theoretical prediction based on Eq. (7) are also plotted.

The R-curves for the composites containing 15 vol% dispersoid are plotted in Fig. 2(a), in which the dependence of the crack resistance (K_R) upon crack extension (Δa) from the root of the notch is presented. The K_R value plotted at $\Delta a = 0$ (usually indicated as K_{I0}) is that corresponding to the load at which the load-displacement curves diverge from a linear trend. SEM observation confirmed that in all the composites a subcritical crack extension of a few tens of microns had occurred very quickly and detectably below the maximum load. Because of its sudden character, the initial discontinuous crack extension has been called pop-in crack propagation according to a previous theoretical assessments.[6] The K_{I0} value was similar in both composites, being 3.6 and 3.8 MPa $\sqrt{m}$ for Mo and FeAl, respectively. Linear rising R-curves were found in both composites. The slope of the R-curves, in comparison with that quite low of pure alumina[12,13] (i.e. 1.2 MPa $\sqrt{m}$/mm), was enhanced by the presence of the dispersoids, being 2 and 4.3 MPa $\sqrt{m}$/mm in the case of Mo and FeAl, respectively. In the latter case, the fracture resistance reached the remarkable value of $K_R \approx 9$ MPa $\sqrt{m}$ for a crack propagation of 1 mm.

A different behavior was found for the composites added with 25 vol% (Fig. 2b). A higher Mo fraction produced a more marked rising R-curve behavior. However, increasing the fraction of FeAl in alumina produced a very poor result: the R-curve behavior degradated and became very similar to that of monolithic alumina, showing almost no toughening effects due to the intermetallic dispersoid.

3.2. Residual stresses

Given the difficulty in theoretically assessing residual stresses in ceramic/metal composites, due to both creep during cooling of the ceramic creep and the unknown relaxation effect of the metal on cooling, an experimental approach by fluorescence spectroscopy was adopted in this study. The average residual stresses measured in the alumina matrix were indeed unexpected compared to first approximation estimations based only on the mismatch of CTE's between the constituent phases. For Al_2O_3/M0 (15 vol%) composite, the CTE mismatch suggests that the matrix should be in tension, however, the experimental average stress was compressive and $\cong -40$ MPa. The average stress remained compressive also for 25 vol% addition, but reaching a higher value of $\cong -110$ MPa. In the Al_2O_3 /FeAl composites, the higher thermal expansion coefficient of the intermetallic compared to that of the matrix was the preponderant factor, and the residual stress was indeed compressive ($\cong -120$ MPa) for the 15 vol% added material. However, a tensile (average) residual stress of about 100 MPa was measured in the 25 vol% added sample. Residual stress data for all the composites investigated are summarized in Table 2. We shall show, in the discussion, that these residual stresses can be explained according to a more detailed model which also considers the elastic mismatch. In addition, an attempt to relate the residual stresses to the toughening behavior will be also shown.

Table 1
Miscellaneous of physical and mechanical properties of the constituent phases of the investigated composites

Materials	Density ρ (g/cm^3)	Young modulus E (GPa)	Poisson ratio ν	Yield strength σ_y (MPa)	Deformation to failure ε_f (%)	CTE α (10^{-6}/°C)
Al_2O_3	3.97	400	0.27	–	–	7
MO	10.22	340	0.38	690	11	5.4
FeAl	5.56	260	0.31	360	5	19

Table 2
Residual stresses and average value of bridging stresses measured by piezo-spectroscopy technique in the investigated composites

Materials	Residual stress (MPa)	Average bridging stress (MPa)
Al_2O_3/Mo (15 vol%)	−40	42
Al_2O_3/Mo (25 vol%)	−110	110
Al_2O_3/FeAl (15 vol%)	−120	85
Al_2O_3Al/FeAl (25 vol%)	100	10–20

3.3. Bridging stresses

Preliminary SEM observation of the crack profiles revealed the bridging effect by dispersoids. As a general trend, cracks were not bridged by small spherical particles (i.e. size < 2–3 μm), which were easily bypassed. Large Mo particles bridged the crack without showing marked ductility [Fig. 3(a)]. Besides the brittle-like behavior of the Mo particles, fracture of the bridging sites always occurred within the metal particle rather than at the particle/matrix interface. Bridging FeAl particles, were also observed along the crack profiles, although the bridging sites mainly failed at the bridging matrix/reinforcement interface Fig. 3(b).

For measuring the bridging stresses, a crack was stably propagated in a bend bar and then arrested after an extension of several hundred microns, using the bending-bar stabilizer previously described. The specimen was then unloaded and, after placing it under an optical microscope into the Raman apparatus, reloaded (in a jig without stabilizer) at the onset for catastrophic fracture (i.e. critical load P_c). Fluorescence low shifts in the Al_2O_3 matrix were continuously collected along the crack profile (at $P = P_c$). These stresses were typically of a tensile nature and, thus, acting as closure (bridging) stresses on the crack faces. Typical linear maps of the bridging stresses as a function of the abscissa x′ along the crack wake and with origin at the crack tip are shown in Fig. 4(a and b) for the Al_2O_3/25 mol% Mo and Al_2O_3/15 vol% FeAl, respectively. The bridging stresses, in both composites, seem to slightly increase with increasing the distance behind the crack tip reaching a maximum at about 300 μm behind the tip.

In Table 2, the average value of the bridging stresses along the crack wake and the residual stresses are reported for all the composites investigates. The highest (average) bridging stress was measured in the 25 vol% of Mo-reinforced composite, and reached 110 MPa. This material also showed the steepest rising R-curve behavior, while the lowest bridging stress was measured in the 25 vol% of FeAl-reinforced material whose fracture behavior was very close to that previously measured in monolithic alumina.[13]

4. Discussion

4.1. Effect of residual stress on toughening

A mechanism which can contribute (positively or negatively) to toughening of ceramic–matrix composites is the thermal residual stress field due to a CTE mismatch between the matrix and the dispersoid. Virkar and Johnson[14] postulated a periodic tension–compression residual stress field when both a CTE and an elastic mismatch between matrix and dispersoid are present in a composite cooled to room temperature. The total

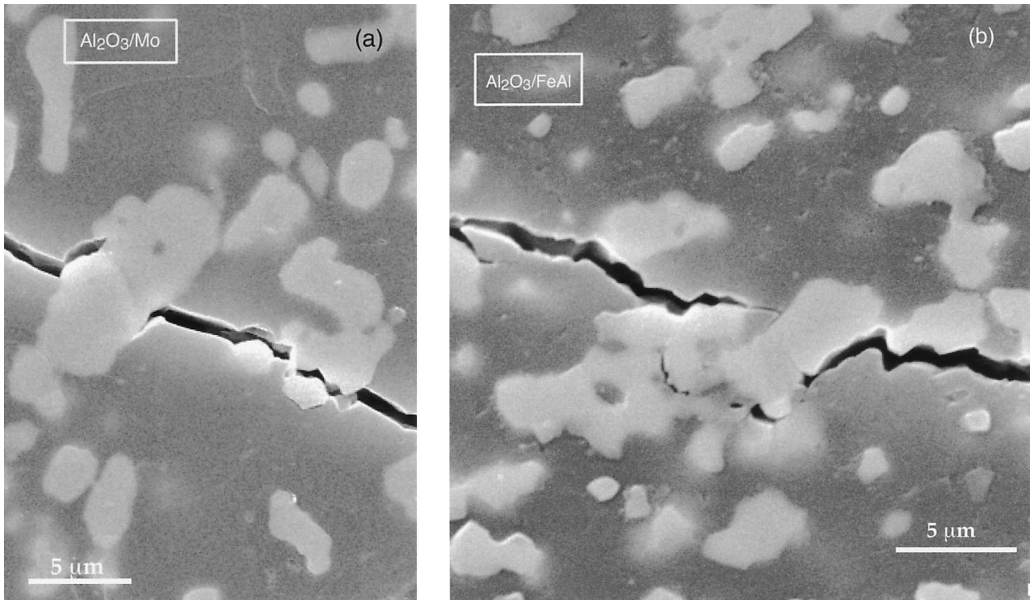

Fig. 3. SEM micrographs of composites showing a different fracture behaviour at the matrix/dispersoid interface: (a) Al_2O_3/Mo, (b) Al_2O_3/FeAl.

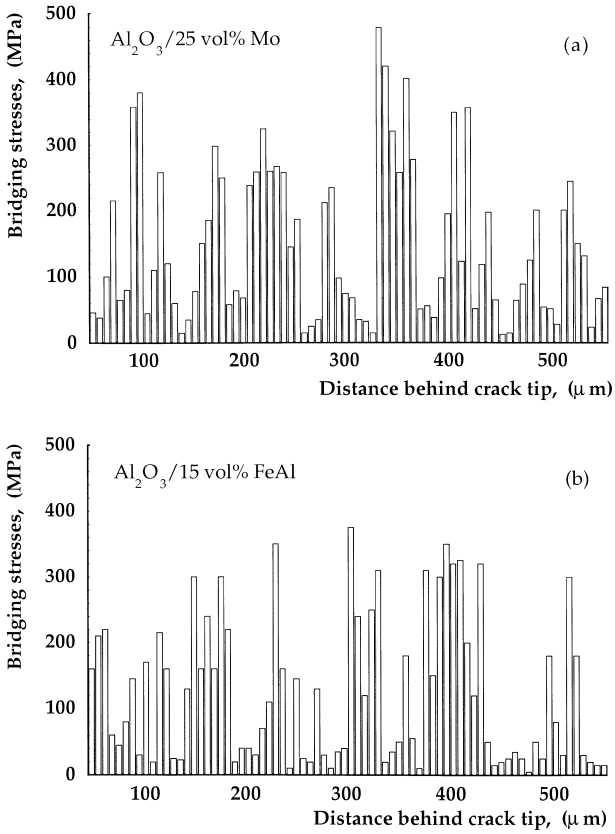

Fig. 4. Map of local closure stresses: (a) Al_2O_3/Mo, added with 25 vol% of Mo, (b) Al_2O_3 added with 15 vol% of FeAl.

stress at any point of the matrix is given by the sum of two terms: a uniform average stress, σ_m, and a locally fluctuating stress component, developed by the neighboring particles, σ_{fl}.[15,16] The uniform average stress, σ_m is given by:

$$\sigma_m = \frac{2\beta f \Delta\alpha \Delta T E_m}{(1-f)(\beta+2)(1+\nu_m)+3\beta f(1-\nu_m)} \quad (1)$$

where f is the dispersoid volume fraction and:

$$\beta = \frac{(1+\nu)E_d}{(1-2\nu_m)E_m} \quad (2)$$

while the fluctuating stress component can be calculated as:

$$\sigma_{fl} = \frac{\beta\Delta\alpha\Delta T E_m\left[\frac{D}{(\lambda-D)} - \frac{D^3}{(2\lambda-D)(\lambda-D^2)}\right]}{2[(1+\nu_m)(\beta+2)]} \quad (3)$$

where, $\Delta\alpha$ is the CTE mismatch, E the Young modulus, ν the Poisson ratio, D the dispersoid size, and the subscripts m and d refer to the matrix and dispersoid, respectively; ΔT is the difference between the hot-pressing temperature and the room temperature, and λ is the interparticle distance which, for spherical particles, can be expressed as:[17]

$$\lambda = D\left(\frac{\pi}{6f}\right)^{1/3} \quad (4)$$

From the above Eqs. (1)–(4), it is clear that there are many factors which influence thermal residual stresses in the composites, not only the CTEs mismatch and ΔT but also, and in a substantial way, the reinforcement/matrix stiffness ratio, their Poisson's ratio, the volume fraction, size of the dispersoid. The load is distributed very unevenly between the metal inclusions, and neighboring inclusions give a non negligible contribution to the stress field. In Figs. 5 and 6, are shown the uniform average stresses, σ_m, in the matrix, the fluctuating stresses, σ_{fl}, and the total stress $\sigma_t = \sigma_m + \sigma_{fl}$, as a function of dispersoid volume fraction, for Al_2O_3/Mo and Al_2O_3/FeAl, respectively. As it can be seen, the average matrix stress is predicted to be slightly in tension when fractions 15 or 25 vol% of Mo are present and in compression when FeAl is added. In addition, the fluctuating stress component is almost zero up to 15 vol% of either Mo or FeAl, although it reaches a compressive value of about −100 MPa at 25 vol% of Mo and a high tensile value of 500 MPa for 25 vol% addition of FeAl. The order of magnitude and the sign of the calculated total residual stresses are both in good agreement with the stresses in the matrix experimentally determined by fluorescence spectroscopy (also indicated in Figs. 5 and 6).

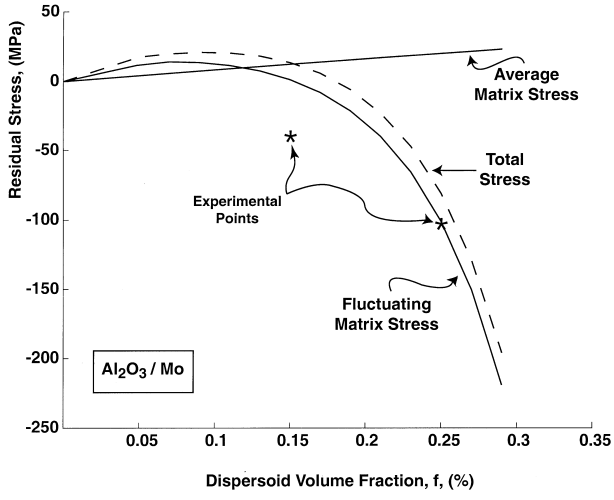

Fig. 5. Theoretical prediction of matrix average and the fluctuating thermal stress as a function of reinforcement volume fraction for the Al_2O_3/Mo composites. The total predicted stress is also shown in comparision with experimental data.

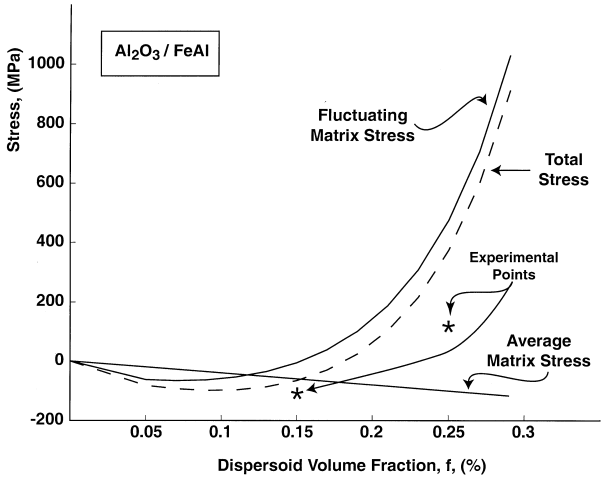

Fig. 6. Theoretical prediction of matrix average and the fluctuating thermal stress as a function of reinforcement volume fraction for the Al_2O_3/FeAl composites. The total predicted stress is also shown in comparision with experimental data.

The toughness change due to residual stresses can be calculated as follows:[16]

$$\Delta K = (\sigma_m + \sigma_{fl})\left(\frac{8\lambda}{\pi}\right)^{1/2} \quad (5)$$

A plot of the relative toughness change, $(K_m + \Delta K)/K_m = K_c/K_m$, predicted according to Eq. (5) is given in Fig. 7, where K_m and K_c are the toughness of the matrix and that of the composite, respectively. As seen, for Mo reinforcement, amounts larger than 20 vol% will produce a positive effect on toughness to increase the matrix value, while almost no effect on toughness is found for lower Mo fractions. In the case of FeAl, only relatively small amounts of reinforcements (less than 18 vol%) will produce a toughness increase. For example, 25 vol% of FeAl will produce a significant embrittlement of the composite.

More in general, for Mo addition, the residual stress effect produces a monotonic increase in toughness as the metal volume fraction increases. In the case of FeAl dispersoid there is an increase in toughness for $f < 20$ vol% but above that fraction, toughness decreases dramatically and, at 25 vol% of FeAl addition, the composite toughness is predicted to be even slightly lower than that of the Al_2O_3 matrix. The effect of a pre-existing stress field on the crack propagation resistance in the composite is mainly exploited at the crack tip, namely, it predominantly affects the K_{I0} of the composite. The experimental K_{I0} values of various composites are plotted in Fig. 7, in comparison with the theoretical predictions. It is noteworthy that, despite the simplified assumption of a residual stress field, theoretical arguments can be provided to justify the monotonic K_{I0} increase of alumina based materials upon increasing the added Mo fraction, as well as their embrittlement upon addition of fraction > 20 vol% of FeAl.

From Figs. 5 and 6, it is also clear that when 25 vol% Mo is added to Al_2O_3 no significant residual stresses are developed. Similar arguments can be given for Al_2O_3 containing 15 vol% FeAl. Therefore, the rising R-curve behavior of these materials should be reasonably explained only on the base of their respective crack-wake bridging stress distributions.

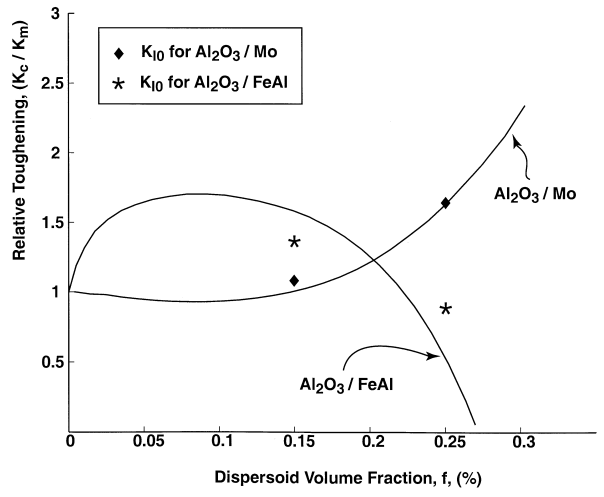

Fig. 7. Theoretical prediction of toughness variation due to residual thermal stresses as a function of the reinforcement volume fraction.

4.2. Effect of bridging stress on toughening

The R-curve contribution arising from the bridging traction, σ_{br}, can be more precisely computed from the knowledge of the bridging stress distribution according to the equation valid for slit cracks:[18]

$$K_R = K_{I0} + \left(\frac{2}{\pi}\right)^{1/2} \int_0^{\Delta a} \frac{\sigma_{br}(x)}{x^{1/2}} dx \quad (6)$$

where $\sigma_{br}(x)$ is the bridging stress distribution over the crack extension Δa and the variable x, with origin at the crack tip, locates the source point for the bridging stress, $\sigma_{br}(x)$. Eq. (6) can be modified to take into account the discrete stress distribution determined by microprobe fluorescence spectroscopy:

$$K_R = K_{I0} + \left(\frac{2}{\pi}\right)^{1/2} \sum_{j=0}^{n} \int_{x_j}^{x_{j+1}} \frac{\sigma_{BR}(x'_j) dx'}{x'^{1/2}} \quad (7)$$

Numerical integration of Eq. (7), performed with using the discrete stress distribution in Fig 4(a and b), leads to the calculated curves reported in Fig. 2(a and b). The results of this calculation fit with good approximation,

the experimental data, for both the Mo- and FeAl reinforced composites, confirming that the main effect on toughening in the present alumina-based materials is provided by crack-face bridging

5. Conclusions

The room-temperature fracture behavior of alumina containing 15 or 25 vol% of either Mo or FeAl dispersoids was investigated by measuring their fracture toughness and rising R-curve behavior. A piezo-spectroscopy technique was employed to evaluate both the residual and the bridging stresses. The outcomes of this investigation can be summarized as follows:

(i) If Mo is used as toughening phase, increasing amounts of metal produce a monotonic increase in toughness and rising the R-curve behavior of the composite. On the other hand, if FeAl is used, embrittlement is found at relatively large volume fractions of intermetallic dispersoid.

(ii) The residual stresses in Al_2O_3/Mo composites are compressive in the matrix and monotonically increasing with the fraction of metal added. On the other hand, the residual stresses in the matrix of Al_2O_3/FeAl composites are compressive when 15 vol% of second phase is present, but they become tensile when 25 vol% is added. This residual stress behavior is considered to produce the embrittlement (i.e. $K_c < K_m$) experimentally found in this composite.

(iii) A theoretical R-curve trend could also be calculated from the experimental bridging stress distribution, assessed by in situ piezo-spectroscopy, for materials with negligible residual stress. The plot of these theoretical trends lies very close to the respectively measured R-curve behavior.

Acknowledgements

One of the authors (O.S.) acknowledges the financial support, from the Italian National Research Council (CNR) under the grant PF MSTA II. Mr. H. Okuda is acknowledged for his help in the experimental procedures.

References

1. Erdogan, Z. and Joseph, P. F., Toughening of ceramics through crack bridging by ductile particles. *J. Am. Ceram. Soc.*, 1989, **72**(2), 262–270.
2. Evans, A. G., The new high toughness ceramics. In *Materials Science Research*, Vol. 6, ed. J. A. Pask and A. G. Evans. Plenum Press, New York, 1987, pp. 775–794.
3. Ravichandran, S., The mechanics of toughness development in ductile phase reinforced brittle matrix composites. *Acta Metall. Mater.*, 1992, **40**(5), 1009–1022.
4. Kotoul, M., On the shielding effect of a multiligament zone of a crack in WC-Co. *Acta Metall. Mater.*, 1997, **45**(8), 3363–3376.
5. McKamey, C. G., Norton, J. A. and Liu, C. T., Effect of chromium on properties of Fe_3Al. *J. Mater. Res.*, 1989, **4**, 1156.
6. Pezzotti, G., Suenobu, H., Nishida, T. and Sbaizero, O., Measurement of microscopic bridging stresses in alumina/molybdenum composite by in situ fluorescence spectroscopy. *J. Am. Ceram. Soc.*, 1999, **82**(5), 1257–1262 .
7. Nojima, T. and Nakai, O., Stable crack extension of an alumina ceramic in three-point bending test. *J. Soc. Mater. Sci. Jpn.*, 1993, **42**(475), 412–418 .
8. Nishida, T., Hanaki, Y., Nojima, T. and Pezzotti, G., Measurement of rising R-curve behavior in toughened silicon nitride by stable crack propagation in bending. *J. Am. Ceram. Soc.*, 1995, **78**(11), 3113–3116.
9. Nishida, T., Hanaki, Y. and Pezzotti, G., Effect of notch-root radius on the fracture toughness of a fine-grained alumina. *J. Am. Ceram. Soc.*, 1995, **77**(2), 606–608.
10. Forman, R. A., Piermarini, G. J., Barnett, J. D. and Block, S., Pressure measurement made by the utilization of ruby sharp line luminescence. *Science*, 1972, **176**, 284–285.
11. He, J. and Clarke, D. R., Determination of the piezospectroscopic coefficients for chromium-doped sapphire. *J. Am. Ceram. Soc.*, 1995, **78**(5), 1347–1353.
12. Pezzotti, G., Okamoto, Y., Nishida, T. and Sakai, M., On the near-tip toughening by crack-face bridging in particulate and platelet-reinforced ceramics. *Acta Mater*, 1996, **44**(3), 899–914.
13. Pezzotti, G., Sbaizero, O., Sergo, V. and Nishida, T., In situ measurements of frictional/bridging stresses in alumina using Raman spectroscopy. *J. Am. Ceram. Soc.*, 1998, **81**(1), 187–192.
14. Virkar, A. V. and Johnson, D. L., Fracture behaviour of ZrO_2-Zr composites. *J. Am. Ceram. Soc.*, 1977, **60**(11–12), 514–519.
15. Mori, T. and Tanaka, K., Average stress in matrix and average energy of materials with misfitting inclusions. *Acta Metall.*, 1973, **21**, 571–574.
16. Taya, M., Hayashi, S., Kobayashi, A. S. and Yoon, H. S., Toughening of a particulate-reinforced ceramic-matrix composite by thermal residual stress. *J. Am. Ceram. Soc.*, 1990, **73**(5), 1382–1391.
17. Underwood, E. E., In *Quantitative Stereology*, Addison-Wesley Publ., Reading, Massachussets, 1970.
18. Irwin, G. R., Fracture. In *Handbuch der Physik*, Vol. 6, Springer-Verlag, Berlin, 1958, pp. 551–5940.